Technical Notes

TECHNICAL NOTES are short manuscripts describing new developments or important results of a preliminary nature. These Notes cannot exceed 6 manuscript pages and 3 figures; a page of text may be substituted for a figure and vice versa. After informal review by the editors, they may be published within a few months of the date of receipt. Style requirements are the same as for regular contributions (see inside back cover).

AIAA 81-4228

Regular to Mach Reflection Transition in Truly Nonstationary Flows—Influence of Surface Roughness

K. Takayama*
Tohoku University, Sendai, Japan
G. Ben-Dor†
Ben-Gurion University of the Negev, Beer-Sheva, Israel
and
J. Gotoh‡
Tohoku University, Sendai, Japan

Introduction

THE reflection of oblique shock waves is a nonlinear problem which has been investigated analytically and experimentally by many researchers. The recent publications concerning this problem have indicated that, in general, the phenomenon of shock-wave reflection should be divided into three cases, according to the type of flow, i.e., 1) steady flow, 2) pseudosteady flow, and 3) truly nonstationary flow.

The reflections possible in each type of flow, as well as the appropriate transition criteria between them, are described by Ben-Dor and Glass[1,2] for a pseudosteady flow, Ben-Dor[3] for a steady flow, and Ben-Dor et al.[4] for a truly nonstationary flow.

It has been shown in Ref. 4 that in truly nonstationary flows (i.e., flows that cannot be made pseudosteady) the transition point from regular (RR) to Mach reflection (MR) is different from the transition point from MR to RR, that is, a hysteresis loop exists in the RR⇌MR transition in truly nonstationary flows.

As a further step, in the course of the study of the transition in truly nonstationary flows, it was decided to investigate the effect of surface roughness on the MR→RR and the RR→MR transition points. The MR→RR transition was obtained by using a concave wedge and the RR→MR transition was obtained by using a convex wedge, see Ref. 4 for details. It is found that in both transitions in concave and convex wedges, the critical transition angles become smaller with increasing surface roughness as compared to curved smooth wedges.

Experiments and Results

Each model (convex or concave) was investigated with three different degrees of surface roughness: 1) smooth surface, 2) mesh No. 320 sand paper, and 3) mesh No. 40 sand paper. Practically, a sand paper of mesh No. X is defined as follows: all the grains of mesh X roughness can pass through a mesh having the size 25.4 mm/X. Therefore, the average roughness for mesh 320 sand paper is 0.08 mm, and 0.6 mm for mesh 40 sand paper. The thicknesses of the sand papers were 0.3 mm for mesh 320 and 1.3 mm for mesh 40. The sand papers were carefully attached to the model surface by epoxy resin.

The experiments were conducted in the 4×8-cm conventional shock tube.[5] Two types of curved wedges were used. The concave cylinder 50 mm in radius, increased from 0 to 90 deg and the convex cylinder 40 mm in radius, decreased from 90 to 0 deg. Consequently, while the MR→RR transition takes place over the concave wedge, the RR→MR transition occurs over the convex model.

The incident shock Mach number range was $1.1 < M_s < 4.0$. The shock-wave velocity was measured with pressure transducers (Kistler Model 606) and a digital counter (Iwatsu UC 7641) and a transient recorder (Iwatsu DM 901). The pressure transducers were located 120 mm apart just ahead of the test section. The effects of attenuation or acceleration of the incident shock waves were examined in the preparatory experiments and found negligible.

Dry air at initial pressures of $3 < P_0 < 150$ Torr was used as a test gas. Ben-Dor[6] has shown that in the range $M_s < 6$ the initial pressure does not influence the RR⇌MR transition. Consequently, the initial pressure could be considered practically constant. The initial temperature T_0 was nearly 300 K throughout the experimental study.

The nonstationary phenomena were observed using shadowgraphs and double exposure holographic interferometric photographs. A giant-ruby laser with a light pulse width of 20 ns was used as an instantaneous light source. In order to observe the wave interaction process continuously, an Ima-Con high-speed camera (John Hadland model 700) was used in both the framing and streak modes. In the streak mode operation, 0.6 mm wide curved slits (for the concave wedge) and 0.7 mm wide curved slit (for the convex wedge) were placed accurately on the test section window in a direction that coincides with the curved wedge surface. These slits were used only for the curved wedges with smooth surface and mesh 320 surface roughness. In this arrangement the transition points along the curved wedges could be determined easily and accurately for each experiment, see Ref. 4 for details. For mesh 40 surface roughness, a wider curved slit was used since the grain size was larger. In addition to this, as seen in Fig. 1, the boundary of the change of the wave interaction patterns were diffused due to the larger surface roughness. Consequently, the measured transition angles include an uncertainty of ±1.0 deg.

Typical interferometric photographs of a RR over a convex wedge with mesh 40 surface roughness and a MR over a concave wedge with mesh 40 surface roughness are shown in Figs. 1a and 1b for $M_s = 1.5$. The comparison of these two photographs with those shown in Fig. 2, for smooth surfaces, indicates that the mesh 40 surface roughness introduces very strong disturbances into the flow and the wave interaction processes are seen to be highly diffused due to the interaction from the many wavelets or Mach lines generated from the random roughness.

Figure 3 represents the present experimental results (the transition angle θ_{crit} vs ξ where ξ is the inverse of incident shock strength). The solid lines A and B correspond to

Received Sept. 24, 1980; revision received Feb. 25, 1981.

*Associate Professor, Institute of High Speed Mechanics.
†Senior Lecturer, Dept. of Mechanical Engineering. Member AIAA.
‡Graduate Student, Institute of High Speed Mechanics.

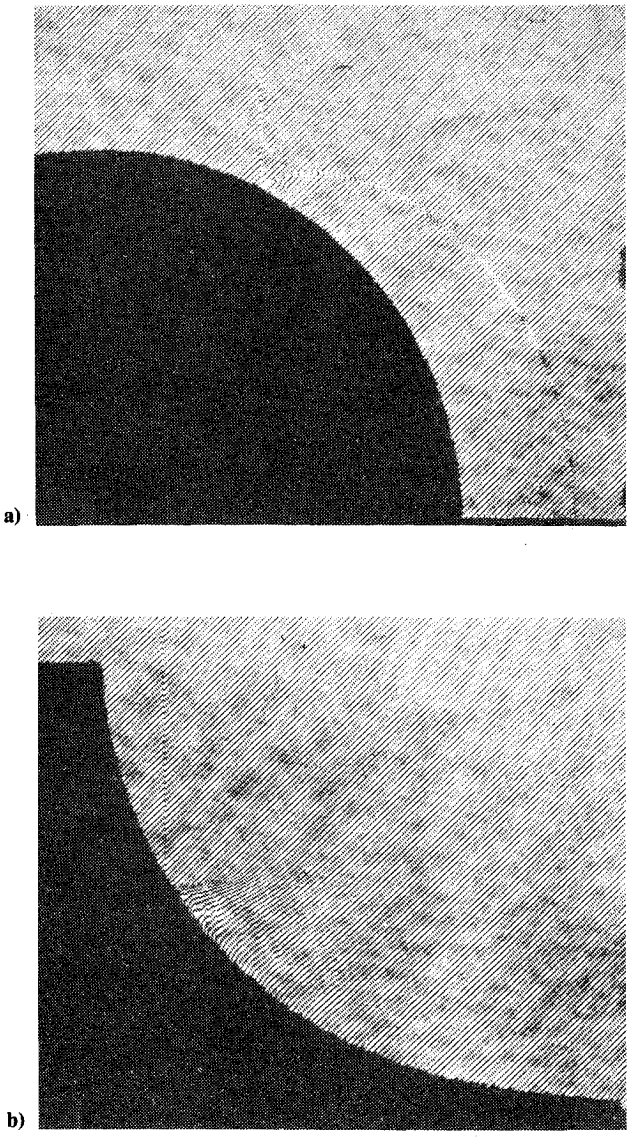

Fig. 1 Typical photographs illustrating shock wave reflection over curved rough surfaces, mesh 40, $M_s \simeq 1.5$; a) regular reflection over a convex wall and b) Mach reflection over a concave wall.

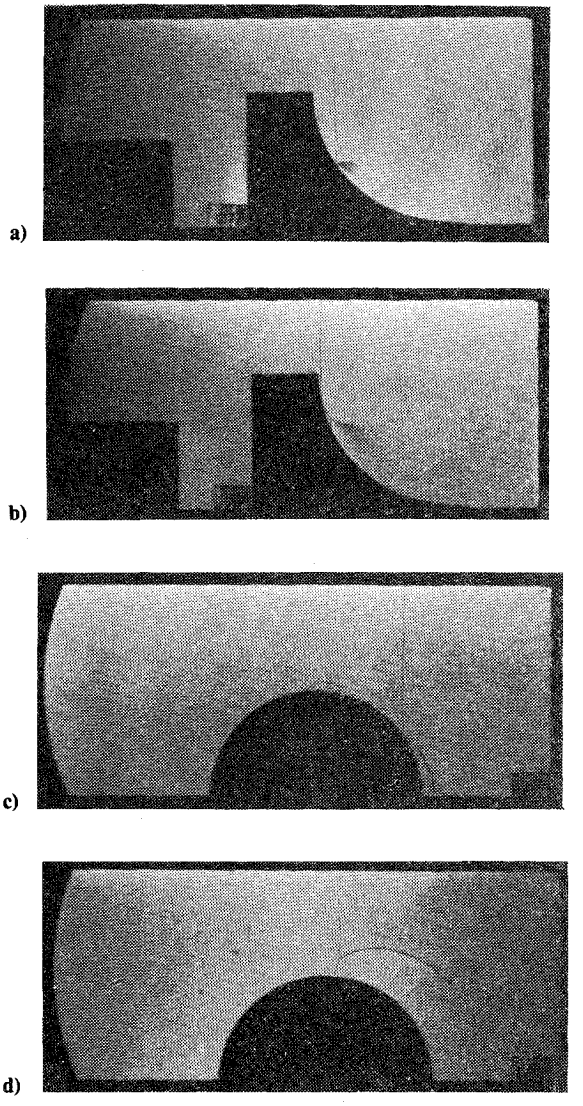

Fig. 2 Instantaneous shadowgraphs illustrating RR and MR, in dry air, at $M_S = 1.40$; a) Mach reflection over a concave wedge, b) regular reflection over a concave wedge, c) regular reflection over a convex wedge, and d) Mach reflection over a convex wedge.

RR⇌MR transition criteria in pseudosteady and steady flows, respectively. The dashed lines indicate the shift in the transition lines due to real gas effects (dissociational equilibrium).

It is seen clearly from Fig. 3, that while the influence of a mesh 320 surface roughness is almost unnoticeable, the mesh 40 surface has a significant effect on the transition angles. At about $M_s = 4$ ($\xi = 0.05$), the transition angles for both the concave and convex wedges are about 10 deg smaller than those corresponding to smooth surfaces. It is clear that the transition angles for both concave and convex wedges decrease with increasing surface roughness. This is due to the fact that the larger surface roughness gives rise to more severe wave interactions or to more significant energy dissipation in the flow.

For the wedges with mesh 40 surface roughness, it seems that the transition point does not depend on the incident shock-wave Mach number for the convex wedge and it depends on the incident shock-wave Mach number very weakly for the concave wedge. Therefore one can conclude from our experiments that in a surface having a roughness equivalent to that of a mesh 40 sand paper the MR→RR transition occurs at about 54 deg and the RR→MR transition takes place at about 27 deg, independent of the incident shock-wave Mach number.

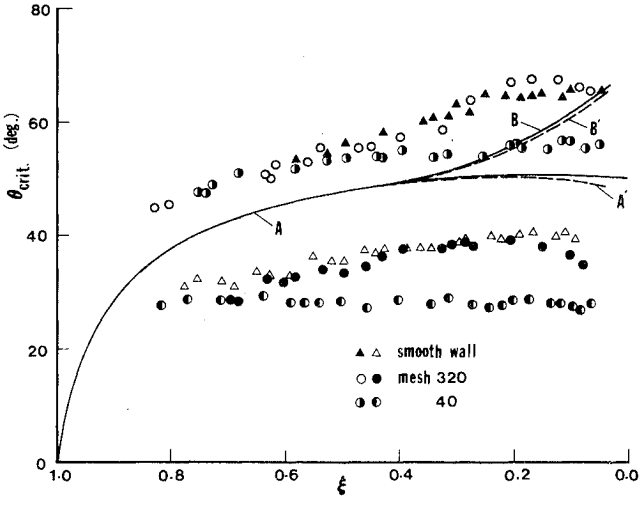

Fig. 3 Present experimental results of actual transition from MR→RR and from RR→MR in the (ξ, θ_w) plane and some theoretical transition lines; ξ, inverse pressure ratio across the incident shock wave; θ_w, wedge angle; (——), perfect diatomic ($\gamma = 7/5$) gas; (---), imperfect nitrogen in dissociational equilibrium; line A, RR⇌MR transition line in pseudosteady flows; line B, RR⇌MR transition line in steady flows.

Conclusions

An experimental investigation of the RR→MR and MR→RR transitions over concave and convex, smooth and rough wedges revealed that 1) as the surface roughness increases, the wedge angle at which transition takes place (for a given Mach number) decreases and 2) for a mesh 40 sand paper type surface roughness, it seems that the transition angle becomes independent of the incident shock wave Mach number, i.e., a) MR→RR transition occurs at $\theta_w \simeq 54$ deg and b) RR→MR transition takes place at $\theta_w \simeq 27$ deg.

These results should be of great importance to those dealing with reflections of blast waves, since this type of problem involves nonstationary flows and high degrees of surface (ground) roughness.

Acknowledgments

The authors would like to express their appreciation to Prof. M. Honda of the Institute of High Speed Mechanics, Tohoku University, Japan for his encouragement throughout the present study. The authors are indebted to Mr. O. Onodera for his help in conducting the present experiments.

References

[1] Ben-Dor, G. and Glass, I. I., "Domains and Boundaries of Nonstationary Oblique Shock Wave Reflexions: 1. Diatomic Gas," *Journal of Fluid Mechanics*, Vol. 92, Pt. 3, June 1979, pp. 459-496.

[2] Ben-Dor, G. and Glass, I. I., "Domains and Boundaries of Nonstationary Oblique Shock Wave Reflexions: 2. Monatomic Gas," *Journal of Fluid Mechanics*, Vol. 96, Pt. 4, Feb. 1980, pp. 735-756.

[3] Ben-Dor, G., "Steady Oblique Shock Wave Reflections in Perfect and Imperfect Monatomic and Diatomic Gases," *AIAA Journal*, Vol. 18, Sept. 1980, pp. 1143-1145.

[4] Ben-Dor, G., Takayama, K., and Kawauchi, T., "The Transition from Regular to Mach Reflection and from Mach to Regular Reflection in Truly Nonstationary Flows," *Journal of Fluid Mechanics*, Vol. 100, Pt. 1, 1980, pp. 147-160.

[5] Takayama, K., Honda, M., and Onodera, O., "Shock Propagation along 90 Degree Bends," Institute of High Speed Mechanics, Tohoku Univ., Vol. 35, 1977.

[6] Ben-Dor, G., "Regions and Transitions of Nonstationary Oblique Shock-Wave Diffractions in Perfect and Imperfect Gases," UTIAS Rept. 232, Aug. 1978.

[7] Takayama, K. and Kawauchi, T., "Shock Diffraction over Concave and Convex Walls," Institute of High Speed Mechanics, Tohoku Univ., Vol. 44, No. 391, 1980.

AIAA 81-4229

Transonic Dip Mechanism of Flutter of a Sweptback Wing: Part II

Koji Isogai*
National Aerospace Laboratory, Tokyo, Japan

IT is well known that a sweptback wing experiences a sharp drop of the flutter boundary in the transonic regime, called the transonic dip phenomenon. A possible mechanism of the phenomenon is presented in Ref. 1. The main conclusion reached in Ref. 1 was that the large time lag between the aerodynamic pressures and the airfoil motion, which is due to the compressibility effect, in the transonic region produces a large negative damping for the first bending mode of a sweptback wing and, thus, the mechanism of a single-degree-of-freedom flutter is dominating at the bottom of the transonic dip when the mass ratio is relatively large. This conclusion was derived from the flutter analysis of a two-dimensional wing having vibrational characteristics similar to a typical streamwise section of a sweptback wing. However, since the unsteady aerodynamic forces employed for the flutter analysis were those predicted by linear subsonic theory,[2] important nonlinear aerodynamic effects such as a shock wave were not taken into account. As pointed out by Ashley,[3] the role of the shock in the transonic flutter of a wing must be of great importance. In view of this, a computer code[4] has been developed to solve the transonic small perturbation (TSP) equation numerically by a finite-difference method. This TSP code can be applied for a wide range of reduced frequency, based on semichord, of $0 \lesssim k \lesssim 0.50$ at transonic Mach numbers from subcritical to above Mach 1. The finite-difference scheme employed in the code is a time-marching semi-implicit and implicit two-sweep procedure. To capture the shock wave, a quasiconservative scheme is employed. Further details of the scheme and the validation of the code are outlined in Ref. 4. The purpose of this Note is to recalculate the flutter boundary of the same binary (bending-torsion) system treated in Ref. 1, this time using the nonlinear aerodynamic forces predicted by the TSP code, and to identify the role of a shock wave in the transonic dip phenomenon.

The airfoil considered is a NACA 64A010 (at zero mean angle of attack). In Fig. 1, the mean steady pressure distributions on the airfoil are shown for Mach numbers 0.70, 0.75, 0.775, 0.80, 0.825, 0.85, 0.875, 0.90, and 1.01. In the figure, P and P_0 are the static and stagnation pressures, respectively, and $(P/P_0)^*$ indicates the sonic condition. The flutter boundaries corresponding to these Mach numbers are determined by employing the conventional U-g method. Further details of the present flutter analysis can be found in Ref. 4. The natural vibration modes and frequencies (ω_1 and ω_2) of the binary system used in the present flutter analysis are shown in Fig. 2, where ω_α is the uncoupled frequency in pitch. As pointed out in Ref. 1, the existence of the pivotal point ahead of the leading edge in the first natural mode is one of the key factors in the mechanism of the transonic dip. The x coordinate of the pivotal point x_{pv} (percent semichord, minus toward the leading edge) is -3.87 for the first natural mode and -0.13 for the second. The calculated flutter velocity coefficients $U_F/(b\omega_\alpha\sqrt{\mu})$ (where U_F is the flutter velocity, b the semichord, and μ the mass ratio) for $\mu = 60$ are also plotted in Fig. 2 as a function of Mach number and compared with those predicted by the linear aerodynamic theory [doublet-lattice method (DLM)[2]]. (At $M_\infty = 0.875$, the periodic solution of the unsteady aerodynamic forces has not been obtained, although the solution is numerically stable. Therefore, the flutter points at $M_\infty = 0.85$ and 0.90 are connected by the dotted line.) As seen in Fig. 2, a sharp transonic dip of the flutter boundary is predicted when the nonlinear aerodynamic forces (TSP code) are used. (The exact agreement of the TSP results with those of the DLM at $M_\infty = 0.70$ seems to be fortuitous since there still exists some effect of the airfoil thickness in the aerodynamic forces even for $M_\infty \lesssim 0.70$.) When looking at the mean steady-pressure distributions shown in Fig. 1 and the sonic line and shock-wave patterns shown in Fig. 2, it is noted that the behavior of the shock wave vs Mach number has a close relation with the behavior of the flutter boundary. (The vertical scale of the sonic line pattern at $M_\infty = 0.90$ is reduced somewhat for illustration purposes.) At Mach numbers 0.825 and 0.85, when the flutter speed takes a minimum value, the shock wave is located at 60% chord position at $M_\infty = 0.825$ and 75% chord position at $M_\infty = 0.85$, respectively, on the airfoil. However, at $M_\infty = 0.90$, when the flutter speed increases abruptly to a value six times that at $M_\infty = 0.825$ and 0.85, the

Received Sept. 26, 1980; revision received March 19, 1981.

*Senior Researcher. Member AIAA.